C. R. Palevol 15 (2016) 209–226

Contents lists available at ScienceDirect

Comptes Rendus Palevol

www.sciencedirect.com

General Palaeontology, Systematics and Evolution

Enamel thickness and enamel growth in *Oreopithecus*: Combining microtomographic and histological evidence

Épaisseur et croissance de l'émail chez Oreopithecus *: combinaison de données microtomographiques et histologiques*

Clément Zanolli[a,*], Christopher Dean[b], Lorenzo Rook[c], Luca Bondioli[d], Arnaud Mazurier[e,f], Roberto Macchiarelli[g,h]

[a] *Multidisciplinary Laboratory, The "Abdus Salam" International Centre for Theoretical Physics, Trieste, Italy*
[b] *Department of Cell and Developmental Biology, University College, London, UK*
[c] *Dipartimento di Scienze della Terra, Università di Firenze, Firenze, Italy*
[d] *Sezione di Bioarcheologia, Museo Nazionale Preistorico Etnografico "Luigi Pigorini", Rome, Italy*
[e] *Société études recherches matériaux, Poitiers, France*
[f] *Institut IC2MP, UMR 7285 CNRS, Université de Poitiers, Poitiers, France*
[g] *Département de Préhistoire, UMR 7194, Muséum national d'Histoire naturelle, Paris, France*
[h] *Département Géosciences, Université de Poitiers, Poitiers, France*

ARTICLE INFO

Article history:
Received 16 November 2014
Accepted after revision 3 February 2015
Available online 17 June 2015

Keywords:
Oreopithecus bambolii
Late Miocene
Dental structure
Virtual paleodontology
Tooth histology
Life history traits

ABSTRACT

Oreopithecus bambolii, a large-bodied fossil ape, lived in the Tusco-Sardinian archipelago during the Late Miocene, until ca. 6.7 Ma. Its dentition, an apparent blend of hominoid and cercopithecoid-like features, has been a matter of discussion since its first description, in 1872. While the height and sharpness of its molar cusps recall some Cercopithecidae, *Oreopithecus* is currently considered by many as more likely related to dryopithecines. Here, we use microtomographic-based quantitative imaging and histological evidence to link outer and inner tooth structural morphology with enamel development in *Oreopithecus* permanent teeth. The material consists of 14 teeth/crowns from the sites of Baccinello and Casteani, in Tuscany, and Fiume Santo, in Sardinia. In particular, we add to the record of 2–3D of molar enamel thickness topographic variation and enamel-dentine junction morphology, and using high-resolution replicas of the outer crown and ground sections, comparatively assess molar growth trajectory (crown formation times and enamel extension rates). Our results shed new light on dental development of this "enigmatic anthropoid" and provide additional evidence concerning the still debated question of its evolutionary history.

Mots clés :
Oreopithecus bambolii
Miocène supérieur
Structure dentaire
Paléodontologie virtuelle
Histologie dentaire
Traits d'histoire de vie

RÉSUMÉ

Oreopithecus bambolii est un grand singe fossile qui a vécu dans l'archipel tusco-sarde durant le Miocène tardif, jusqu'à il y a environ 6,7 Ma. Sa denture, un mélange apparent de caractéristiques similaires à celles des hominoïdes et des cercopithécoïdes, a été sujet à discussions depuis sa première description en 1872. Tandis que la hauteur et l'aspect saillant des cuspides des molaires rappellent ceux de certains Cercopithecidae, *Oreopithecus* est actuellement considéré par beaucoup comme étant très probablement lié aux

* Corresponding author.
E-mail address: clement.zanolli@gmail.com (C. Zanolli).

http://dx.doi.org/10.1016/j.crpv.2015.02.001
1631-0683/

dryopithécinés. Nous exploitons ici des données quantitatives basées sur l'imagerie microtomographique et histologique pour relier la morphologie structurale externe et interne des dents permanentes avec le développement de l'émail chez *Oreopithecus*. Le matériel comprend 14 dents/couronnes provenant des sites de Baccinello et Casteani, en Toscane, et de Fiume Santo, en Sardaigne. Plus précisément, nous combinons au registre 2–3D des variations topographiques de l'épaisseur de l'émail et de la morphologie de la jonction émail-dentine des molaires, des moulages haute résolution de la surface externe de la couronne et des sections histologiques, et nous estimons comparativement la trajectoire de croissance des molaires (temps de formation de la couronne et taux d'extension de l'émail). Nos résultats apportent un nouvel éclairage sur le développement dentaire de cet « anthropoïde énigmatique » et fournissent des informations supplémentaires concernant la question toujours débattue de son histoire évolutive.

1. Introduction

Oreopithecus bambolii, named by the French paleontologist P. Gervais (1872), is a Late Miocene large-bodied hominoid endemic to the northern Tyrrhenian area (Tusco-Sardinian paleobioprovince; Rook et al., 2006). It is known from several localities in southern Tuscany (Acquanera, Baccinello, Casteani, Monte Bamboli, Montemassi, Ribolla; Benvenuti et al., 2001) and one site in northern Sardinia (Fiume Santo; Abbazzi et al., 2008; Casanovas-Vilar et al., 2011a; Cordy and Ginesu, 1994). Although its phylogenetic relationships with respect to the European dryopithecines are still debated (Alba, 2012; Begun, 2002; Casanovas-Vilar et al., 2011a; Harrison and Rook, 1997; Moyà-Solà and Köhler, 1997; Wood and Harrison, 2011), *Oreopithecus* is widely considered an ape displaying a blend of primitive, derived and unique features (Köhler and Moyà-Solà, 1997; Rook et al., 1999). It is one of the rare hominoids that persisted in Europe after the Vallesian Crisis (Casanovas-Vilar et al., 2011b; Rook et al., 2011; Spassov et al., 2012), and its evolution in an insular context until ca. 6.7 Ma was likely responsible for the development of a number of craniodental morphological peculiarities and adaptations (Köhler and Moyà-Solà, 2003; Moyà-Solà and Köhler, 1997) which are unique to this "enigmatic anthropoid" (Delson, 1986).

Oreopithecus post-canine teeth display high, voluminous bunodont cusps linked together by a number of crests (e.g., the mid-trigonid crest, the oblique crest linking the metaconid with the hypoconid, the hypolophid, the postcristid) and some accessory cusps (e.g., paraconid, protoconulid, centroconid) (Butler and Mills, 1959; Harrison and Rook, 1997). However, the structural relationships between its complex occlusal morphology and the features expressed at the dentine level remain poorly known (Zanolli et al., 2010). In addition, insular environments often lead to accelerated life history schedules and a number of morphological traits of the *Oreopithecus* craniofacial and dental complex (e.g., relatively small brain size, reduction of prognathism, low canine crowns and microdontia) have been interpreted as evidence for heterochrony (Alba et al., 2001a,b; Moyà-Solà and Köhler, 1997).

Information available so far on the inner dental structure of this fossil hominoid derives from a few histological sections of molar teeth (Andrews and Martin, 1991; Olejniczak et al., 2004; Smith et al., 2003) and from a preliminary microtomographic-based investigation of a deciduous and a permanent molar (Zanolli et al., 2010). By combining microtomographic and histological evidence, this study aims to identify links between tooth structural morphology and enamel development in *Oreopithecus*. Specifically, we present two- and three-dimensional (2–3D) data on topographic variation in enamel thickness and the morphology of the enamel-dentine junction (EDJ) based on the microtomographic analysis of four *Oreopithecus* molars. We combine this record with original data on enamel growth derived from perikymata counts on surface enamel and histological sections. This allowed the study of enamel formation rates and gradients of enamel formation increasing from the EDJ to the tooth surface.

2. Materials

The *O. bambolii* dental sample considered in this study consists of the permanent upper canine (UC), fourth premolar (UP4) and first to third molars (UM1 to UM3) of the maxillary specimen IGF4332 and the third molar (LM3) of the mandibular fragment IGF4351, both from the site of Casteani (Rossi et al., 2004); the second molar (LM2) from the partial mandible IGF4883 V from Baccinello (Rook et al., 1996); and six isolated crowns from Fiume Santo representing a permanent lower lateral incisor (LI2: FS#BC-23), a lower fourth premolar (LP4: FS#Q16-64), a lower first molar (LM1: FS1996#Fi98), two lower second molars (LM2: FS1996#Fi99 and FS#Q16-59), and a lower third molar (LM3: FS1996#Fi97) (Abbazzi et al., 2008).

Histological analysis was carried out on the LM2 from Baccinello (IGF4883 V) and also on two additional isolated enamel cap fragments (FS#BC-nn), presumably from the same tooth from the Fiume Santo assemblage. These enamel fragments, very likely from a LM2 (or less likely a LP4), measure ~ 7.3 mm and ~ 8.2 mm high from cusp to cervix, respectively, and are both complete from the first-formed cuspal enamel to the last-formed cervical enamel in the longitudinal plane. They were slightly worn over the cusp tip but included a portion of the thick occlusal enamel beyond the tip of the dentine horn. The enamel extending into the occlusal surface of one fragment was

substantial, ~1500 μm thick, supporting its identification as a molar rather than as a premolar fragment. Neither of the two fragments preserved any dentine and so both were completely unsupported beneath the former EDJ.

In order to comparatively assess crown formation times and enamel extension rates, we used published (Dean, 2010) and unpublished evidence (original data from C.D.) on *Pan* and *Gorilla* molars.

The high-resolution microtomographic dental records available to us for representative specimens of the taxa *Homo*, *Pan* and *Gorilla* (Macchiarelli et al., 2008, 2009; Zanolli et al., 2010) were also used to compare the 3D inner structural morphology of the first lower molar (LM1).

3. Methods of analysis

3.1. Microtomographic acquisitions and virtual reconstructions

The LM3 of the mandibular fragment IGF4351 and the three isolated molars FS1996#Fi97 (LM3), FS1996#Fi98 (LM1), and FS1996#Fi99 (LM2) from Fiume Santo were detailed in 2005 by X-ray synchrotron radiation microtomography (SR-μCT) at the ID 17 Beam Line of the European Synchrotron Radiation Facility, Grenoble (experiment SC1749). The scans were performed with an intensity of 200 mA at energies of 51 and 70 keV (for the isolated specimens and the fragments, respectively), with an integration time of 22.6 ms by projections (1500/180°) of 60 ms. Data were collected by a 2.048 × 2.048 fibre-optical taper charge-coupled device Frelon camera (Mazurier et al., 2006). The reconstructions of the sections were saved in a 32-bit floating-point raw format with a voxel size of 45.5 × 45.5 × 45.7 μm.

Using Amira v.5.3 (Visualization Sciences Group Inc.) and ImageJ (Schneider et al., 2012), a semi-automatic, threshold-based segmentation was carried out following the half-maximum height method (HMH; Spoor et al., 1993) and the region of interest thresholding protocol (ROI-Tb; Fajardo et al., 2002) taking repeated measurements on different slices of the virtual stack (Coleman and Colbert, 2007). The specimens were thus digitally reconstructed in 3D using surface rendering allowing the quantification of the enamel cap, the dentine core volume, and the EDJ surface (Fig. 1).

3.2. Enamel thickness virtual assessment

For the specimens detailed by SR-μCT, the scale-free 2D relative enamel thickness (RET; Martin, 1985) was assessed on sections perpendicular to the cervical plane passing through the metaconid-protoconid dentine horns (Fig. 1A). The scale-free 3D relative enamel thickness (3D RET) was computed following Olejniczak et al. (2008a,b,c); (see also, Kono, 2004; Macchiarelli et al., 2006). For the LM3 of IGF4351, the worn enamel apex and dentine horn of the protoconid and the enamel apex of the metaconid were virtually reconstructed for 2D RET using as a reference model the outline of the nearly unworn LM3 FS1996#Fi97 (Fig. 1A), thus allowing a more realistic assessment of its RET value (cf. Zanolli et al., 2010). For this latter specimen, we did not calculate 3D RET.

Linear measurements were taken using the software package MPSAK v.2.9 (available in Dean and Wood, 2003). Intra- and inter-observer tests for accuracy of the 2–3D measurements were run by two observers; recorded differences were less than 4%, which is compatible with similar previous tests (e.g., Macchiarelli et al., 2009).

3.3. Surface replication of specimens

High-resolution silicone moulds of well-preserved enamel surfaces were made on the following specimens: the buccal aspects of the UC and the lingual aspect of the UP4, UM1, UM2 and UM3 of IGF4332; the buccal aspect of the LI2 FS#BC-23, of the LP4 FS#Q16-64 and of the LM2 FS#Q16-59 (Fig. 2). The LM2 of IGF4883 V and the two enamel fragments, FS#BC-nn, were also replicated in this way before proceeding further with sectioning.

The above specimens were replicated using the Coltène President putty and light body wash addition curing silicone impression system. Casts from moulds of these teeth were made in clear epoxy resin and then sputter coated with ~18 nm of gold–palladium to create a reflective surface (Fig. 2). Oblique lighting was then used to illuminate surface perikymata.

3.4. Ground sections

The two enamel fragments, FS#BC-nn, were first embedded in clear epoxy resin (Fig. 3A and B). One initial axial cut was made in the longitudinal plane with a diamond-embedded wafering blade and low speed saw (Buehler, Isomet). One face of the two resulting blocks was then polished and fixed with epoxy resin to a 1 mm thick glass slide. A second parallel axial cut was then made to remove a thin section attached to the glass slide. This was then lapped plane-parallel by hand, polished to ~100 μm thickness, washed, dehydrated in alcohol, cleared in xylene and mounted with a styrene-based (DPX) mounting medium for light microscopy.

The LM2 of IGF4883 V (Fig. 3C) was chosen to provide information about both cervical enamel and root dentine growth. A quadrant was cut from the mesiobuccal root (Fig. 3C) and a ground section prepared as described above. All sections were then examined in polarized transmitted light and photomontages constructed using 125–500 magnification factors.

3.5. Measurement of enamel daily increments

Each of the *Oreopithecus* sections contained regions of daily enamel cross striations that could be measured. Daily average rates in the cuspal regions of the two enamel fragments, FS#BC-nn, were calculated as follows: cuspal enamel thickness was measured from the lateral aspect of the former dentine horn to the surface enamel; these distances were then divided equally into three regions: inner, middle and outer; measurements were made across six consecutive cross striations and then divided by five to give a daily average value. This procedure was repeated 22 times

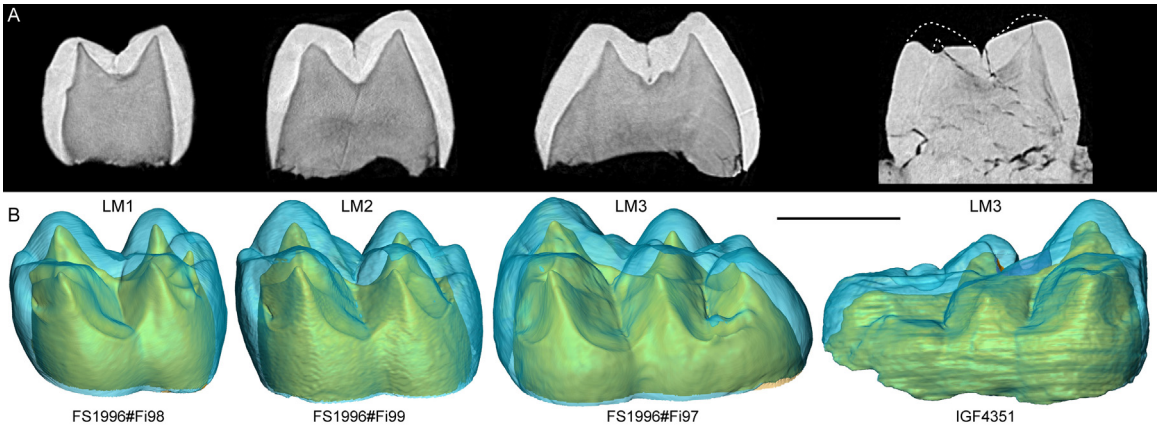

Fig. 1. (Color online.) *Oreopithecus bambolii*. SR-μCT-based sections passing through the mesial dentine horns (A) and 3D virtual renderings (B) of the four permanent lower molars FS1996#Fi98 (LRM1, mirrored), FS1996#Fi99 (LRM2, mirrored), FS1996#Fi97 (LLM3), and IGF4351 (LRM3). All specimens in buccal view with the enamel in semi-transparency. In IGF4351, the worn enamel apex and dentine horn of the protoconid and the enamel apex of the metaconid were virtually reconstructed based on the morphology of the specimen FS1996#Fi97. Scale bar: 5 mm.
Fig. 1. (Couleur en ligne.) *Oreopithecus bambolii*. Sections SR-μCT passant par les cornes de dentine mésiales (A) et rendues virtuelles 3D (B) des quatre molaires inférieures permanentes FS1996#Fi98 (LRM1, inversée), FS1996#Fi99 (LRM2, inversée), FS1996#Fi97 (LLM3), et IGF4351 (LRM3). Tous les spécimens sont en vue buccale avec l'émail en semi-transparence. Pour IGF4351, l'émail et la corne de dentine usés du protoconide, ainsi que le sommet de l'émail du métaconide ont été virtuellement reconstruits en se basant sur la morphologie du spécimen FS1996#Fi97. Échelle : 5 mm.

in the inner, 13 times in the middle, and 20 times in the outer regions of the two sections combined.

Lateral and cervical enamel daily rates were measured in the same fashion within, respectively, the approximate outer mid-third of the crown and the cervical region of IGF4883V.

4. Results

4.1. Outer vs. inner structural morphology

The high-resolution virtual reconstruction of the *Oreopithecus* lower molar crowns (Fig. 1) reveals that each morphological feature expressed at the outer enamel surface (OES) is sharply expressed at the EDJ level (contra Olejniczak et al., 2004). Indeed, while the main cusps are externally well differentiated, the short precingulid accessory cusps (i.e., paraconid, centroconid, tuberculum sextum) and the complex crest network (i.e., the paracristid between paraconid and protoconid, the protocristid between protoconid and metaconid, the hypolophid between hypoconid and entoconid, the hypometacristid between metaconid and centroconid, the hypoprotocristid between protoconid and centroconid, and the entolophid between entoconid and hypoconulid) (Butler and Mills, 1959) are more markedly expressed at the EDJ. In fact, compared to the OES signal, sharper topographic information of taxonomic and phylogenetic value is commonly observed in extant and fossil hominids at the EDJ level (Corruccini, 1987; Macchiarelli et al., 2006, 2009; Olejniczak et al., 2004, 2007; Skinner et al., 2008a,b; Smith et al., 2006, 2009; Zanolli and Mazurier, 2013).

When comparing the OES and EDJ in *Oreopithecus*, *Homo*, *Pan* and *Gorilla* LM1s, the first clearly exhibits a set of unique structural features (Fig. 4). Notably, *Oreopithecus* shows proportionally higher and more slender dentine horns. In addition, instead of having a concave central basin as in extant hominids, it is high and even slightly convex or bulging due to the development of the oblique crest and of the centroconid, which also rise high at the EDJ.

As a whole, based on our 3D comparative record of extant and fossil hominoid lower molars, the degree of structural complexity observed at the EDJ in *Oreopithecus* is unique.

4.2. 2–3D enamel thickness virtual assessment

In the four *Oreopithecus* lower molars imaged by SR-μCT, the thickest cuspal enamel is uniformly found on the buccal aspects of the protoconid and metaconid (Table 1). Similar to the pattern reported for all extant and some fossil hominids (Olejniczak et al., 2008d; Smith et al., 2011, 2012), the *Oreopithecus* specimens investigated here provide evidence for increasing maximal enamel thickness from the LM1, through the LM2, to the LM3. The lingual enamel thickness of the metaconid is nearly uniform, while there is more variation along the protoconid lingual wall.

Similar to *Ouranopithecus macedoniensis* (maximum enamel thickness of the LM1 protoconid: 2.04 mm, metaconid: 1.85 mm; Macchiarelli et al., 2009), the *Oreopithecus* LM1 displays slightly thicker maximum cuspal enamel on the protoconid than on the metaconid. In contrast, the LM2 and LM3 exhibit a more even distribution of the enamel on both cusps (Table 1). This pattern differs from that observed in extant African great apes and *Homo*, where thicker enamel is generally found on the buccal crown side (Grine, 2005; Kono, 2004; Macchiarelli et al., 2009). In the buccolingual section passing through the mesial cusps, *Oreopithecus* maximal radial enamel thickness (1.45 mm) slightly exceeds the measurements available for *Pan* (1.36 mm) and *Gorilla* (1.40 mm), but not the modern human figures (1.89 mm) (in Macchiarelli et al., 2009).

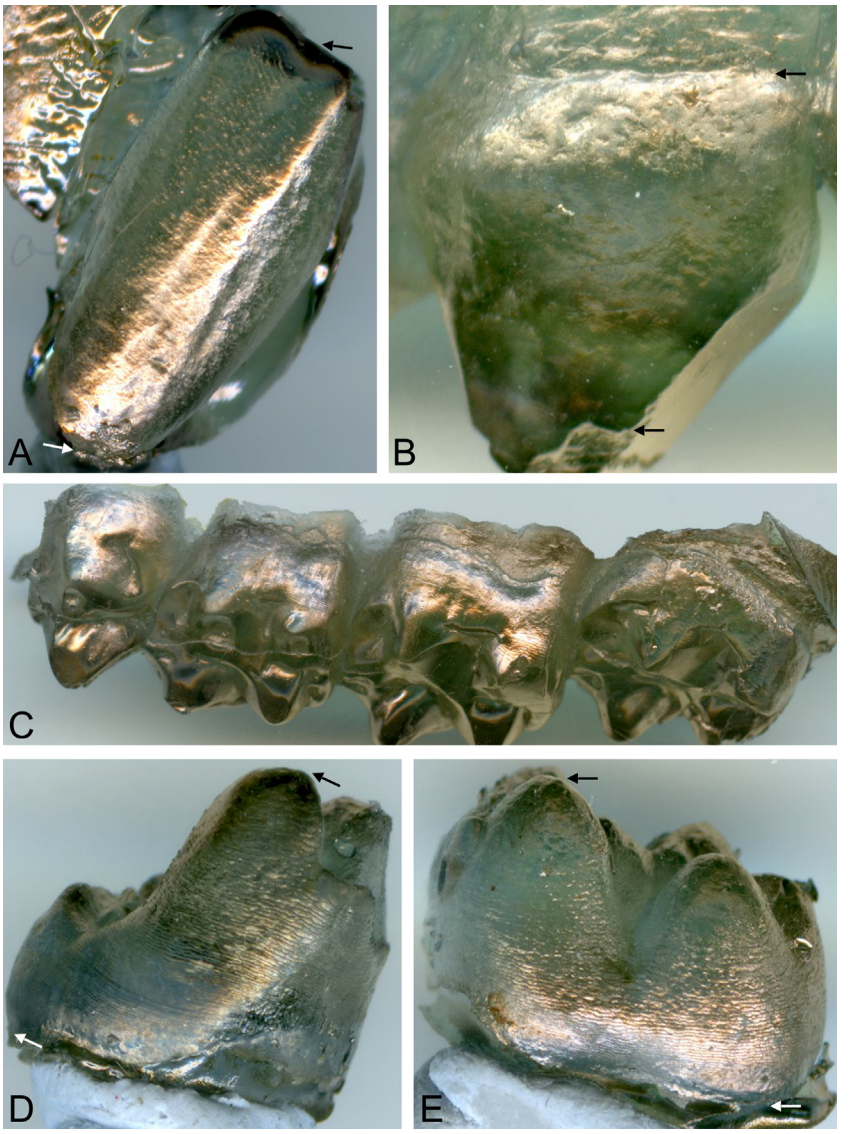

Fig. 2. (Color online.) *Oreopithecus bambolii*. Gold–palladium coated epoxy resin casts of teeth showing the well-preserved perikymata on the lateral crown aspects. A: LI2 (FS#BC-23); B: UC (IGF4332); C: UP4 (to the right) to UM3 (IGF4332); D: LP4 (FS#Q16-64); E: LM2 (FS#Q16-59). The arrows indicate the area where the perikymata could be near-completely counted.
Fig. 2. (Couleur en ligne.) *Oreopithecus bambolii*. Moulages des dents en résine époxyde recouverts d'un alliage or–palladium montrant les périkymaties bien préservées sur l'aspect latéral des couronnes. A : LI2 (FS#BC-23) ; B : UC (IGF4332) ; C : UP4 (à droite) à UM3 (IGF4332) ; D : LP4 (FS#Q16-64) ; E : LM2 (FS#Q16-59). Les flèches indiquent la zone où les périkymaties ont pu être presque intégralement comptées.

Table 1
Maximal cuspal enamel thickness (in mm) in four *Oreopithecus bambolii* lower molars.
Tableau 1
Épaisseur maximale de l'émail (en mm) des cuspides de quatre molaires inférieures chez *Oreopithecus bambolii*.

	FS1996#Fi98	FS1996#Fi99	FS1996#Fi97	IGF4351
Maximal enamel thickness	LM1	LM2	LM3	LM3
Lingual aspect of the metaconid	1.00	0.97	1.00	1.00
Buccal aspect of the metaconid	0.99	1.21	1.45	1.28
Lingual aspect of the protoconid	0.80	1.16	1.22	1.00
Buccal aspect of the protoconid	1.11	1.20	1.41	1.33

Table 2
2D-based relative enamel thickness index (RET) in extant and fossil hominoids (decreasing values). Sample size is reported in parentheses near each taxon.
Tableau 2
Indice 2D d'épaisseur relative de l'émail (RET) chez des hominoïdes actuels et fossiles (valeurs décroissantes). La taille de l'échantillon est indiquée entre parenthèses près de chaque taxon.

Taxon	UM1	UM2	UM3	LM1	LM2	LM3	Mean	Category[t]
Paranthropus robustus (10)[a,b]	28.8		26.8	28.2	35.7		28.5	Hyper-thick
Range	28.6–29.0		22.5–30.3	25.0–30.5				
Ouranopithecus turkae (1)[c]					27.3		27.3	
Ouranopithecus macedoniensis (1)[d]						25.5	25.5	Thick
Range					24.1–24.6			
Australopithecus africanus (11)[b]	21.6	21.3		21.7	23.9	21. 9	22.6	
Range				15.7–27.8	16.5–31.3	17.9–26.8		
Proconsul nyanzae (1)[a]					22.4		22.4	
Gigantopithecus blacki (10)[e]							21.3	
Range								
Afropithecus turkanensis (2)[a]					20.9		20.9	
Range					19.4–22.3			
Homo erectus (Asia) (10)[f,g]	17.7		29.9		22.1	19.9	20.9	
Range	15.8–19.1				18.6–24.9			
Homo heidelbergensis (N Africa) (3)[h,i]		18.8	23.0		17.3	23.4	20.6	
Range								
Early *Homo* (E Africa) (2)[h]	15.6	18.7		21.5	26.2		20.5	
Range								
Homo sapiens (257)[a]	18.8	21.6	21.8	17.0	20.5	21.6	20.1	
Range	14.0–23.9	16.5–28.0	17.0–30.0	11.8–22.6	14.8–27.7	17.2–31.8		
Griphopithecus sp. (8)[a]		19.0		17.2	18.4	22.0	19.3	
Range		17.8–20.2			16.5–20.7	20.9–23.0		
Sivapithecus sivalensis (3)[a]	17.2					20.8	19.2	
Range	16.3–18.2							
Australopithecus africanus (1)[j]						19.1	19.1	
Sivapithecus parvada (1)[a]				18.9			18.9	
Khoratpithecus piriyai (1)[k]					17.6		17.6	
Khoratpithecus chiangmuanensis (2)[l]					17.5		17.5	
Range					17.2–17.8			
Lufengpithecus lufengensis (4)[e]							17.4	
Proconsul heseloni (1)[a]						17.0	17.0	Intermed-thick
Sivapithecus indicus (1)[m]		16.5					16.5	
Neanderthals (42)[n]	15.2	18.1	18.0	15.9	15.7	16.6	16.4	
Range	13.8–16.9	15.7–20.9	14.3–18.9	13.8–16.7	14.2–16.8	15.3–18.3		
Oreopithecus bambolii (5)[a,o,u]	13.0			17.4	17.0	15.8	15.8	
Range						15.1–16.5		
Rangwapithecus gordoni (1)[a]	14.9					14.9	14.9	
Pierolapithecus catalaunicus (5)[p]	14.3	14.5	16.9				14.9	
Range	14.0–14.6	14.4–14.6						
Anoiapithecus brevirostris (7)[p]	14.1	15.2	14.8				14.8	
Range	13.9–14.2	13.0–17.3						
Ardipithecus ramidus (1)[q]	14.8						14.8	

Table 2 (*Continued*)

Taxon	UM1	UM2	UM3	LM1	LM2	LM3	Mean	Category[t]
Pongo pygmaeus (75)[r]	12.3	15.2	16.2	11.8	14.6	16.4	14.3	Intermed-thin
Range	9.0–15.1	10.8–18.2	10.1–22.2	9.7–15.8	11.0–19.5	11.2–22.5		
Lufengpithecus hudienensis (1)[a]				14.1			14.1	
Pongo abelii (44)[r]	12.1	14.0	16.8	12.1	14.2	14.8	13.8	
Range	9.0–16.3	11.2–19.3	12.2–22.1	8.6–14.7	11.2–18.5	9.8–19.1		
Proconsul major (1)[a]						13.7	13.7	
Pan troglodytes (40)[a,s]	10.3	11.4	12.8	12.6	12.9	15.0	13.2	
Range	8.5–12.2	10.7–12.5	10.0–15.0	10.3–14.1	10.9–15.5	13.9–16.6		
Dryopithecus fontani (2)[n]		12.5	13.0				12.7	
Hispanopithecus laietanus (1)[a]	12.7						12.7	
Gorilla gorilla (15)[a,s]	9.8	12.3	10.8	10.8	12.4	13.9	11.7	
Range	9.1–10.1	11.6–13.0	9.8–11.8	9.0–12.6	9.7–15.2	12.8–15.1		
Proconsul africanus (1)[a]	8.5						8.5	Thin

[a] Smith et al. (2006).
[b] Olejniczak et al. (2008c).
[c] Güleç et al. (2007).
[d] Smith et al. (2004).
[e] Zhang and Zhao (2013).
[f] Smith et al. (2009).
[g] Zanolli (2014).
[h] Smith et al. (2012).
[i] Zanolli and Mazurier (2013).
[j] Macchiarelli et al. (2004).
[k] Chaimanee et al. (2006).
[l] Chaimanee et al. (2003).
[m] Mahoney et al. (2007).
[n] Olejniczak et al. (2008a).
[o] Zanolli et al. (2010).
[p] Alba et al. (2013).
[q] Suwa et al. (2009).
[r] Smith et al. (2011).
[s] Smith et al. (2005).
[t] Following Martin (1985).
[u] This study.

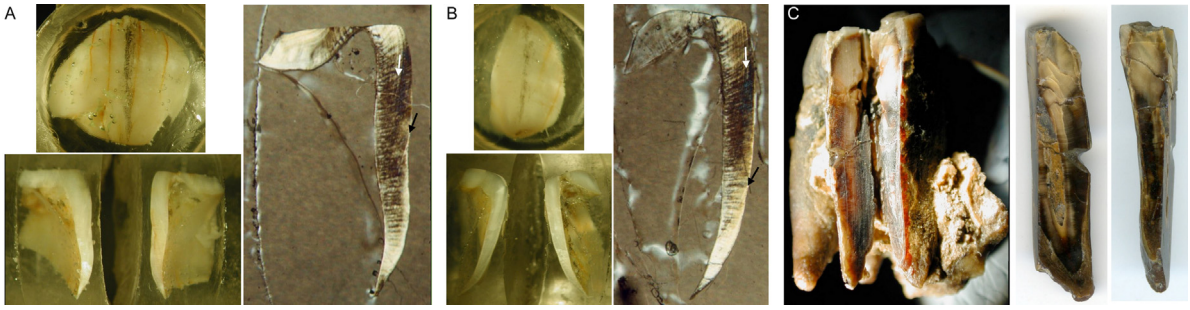

Fig. 3. (Color online.) *Oreopithecus bambolii*. The two enamel fragments FS#BC-nn (A and B) before and after sectioning, and the LM2 IGF4883V (C) with the cut portion of crown and root. The white and black arrows indicate similar accentuated striae in both fragments suggesting they are from the same tooth.
Fig. 3. (Couleur en ligne.) *Oreopithecus bambolii*. Les deux fragments d'émail FS#BC-nn (A et B) avant et après sectionnement et la LM2 IGF4883V (C) avec la portion découpée de la couronne et de la racine. Les flèches blanches et noires indiquent des stries accentuées similaires dans les deux fragments, suggérant qu'ils échantillonnent la même dent.

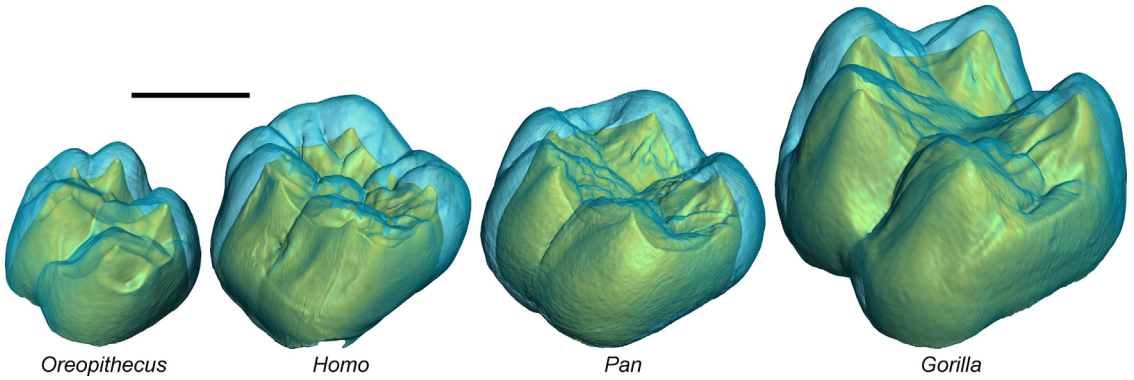

Fig. 4. (Color online.) Comparative virtual rendering (slightly oblique mesiobuccal view) of a permanent lower first molar crown (all right LM1s) in *Oreopithecus* (FS1996#Fi98), *Homo*, *Pan* and *Gorilla*. The enamel is shown in semi-transparency, allowing visualization of the dentine shape. Scale bar: 5 mm.
Fig. 4. (Couleur en ligne.) Comparaison de rendus virtuels (en vue mésio-buccale, légèrement oblique) d'une couronne de première molaire inférieure permanente (toutes des LM1 droites) de *Oreopithecus* (FS1996#Fi98), *Homo*, *Pan* et *Gorilla*. L'émail est montré en semi-transparence, permettant de visualiser la morphologie de la dentine. Échelle : 5 mm.

In order to adjust for size, we calculated both 2D and 3D indices of relative enamel thickness (RET and 3D RET) (Tables 2 and 3).

Previous measures of 2D RET in *Oreopithecus* based on a UM1 physical section (spec. BM-11565) were 13.0 (Smith et al., 2003) and 15.5 (Andrews and Martin, 1991). Based on our results, average 2D RET in *Oreopithecus* lower molars is 15.8, while average 3D RET is 15.6. These estimates near or slightly exceed those reported for members of the Dryopithecinae subfamily, such as *Pierolapithecus catalaunicus*, *Anoiapithecus brevirostris*, *Dryopithecus fontani*, *Hispanopithecus laietanus* (details in Table 2). Conversely, much thicker values characterize the macrodont taxa *Paranthropus robustus*, *Ouranopithecus turkae* and *O. macedoniensis* (Tables 2 and 3). Fossil and extant hominins also tend to display relatively thick enamel (except Neanderthals; Macchiarelli et al., 2007; Olejniczak et al., 2008a). Fossil and extant pongines range from intermediate-thin, in *Pongo abelii*, to thick-enamelled molars, in *Gigantopithecus blacki*, while the African extant great apes *Gorilla* and *Pan* range from thin to intermediate-thin enamel (Tables 2 and 3).

RET values in *Oreopithecus* appear to show an increase in 2D enamel thickness from M3 to M1, i.e., the reverse of the pattern commonly seen in the comparative taxa considered in this study, while the highest 3D RET value was found in the LM2. However, more data from *Oreopithecus* individuals with complete posterior tooth rows are needed to verify this as a taxon-specific characteristic.

4.3. Daily rates of enamel formation, cuspal gradients and cuspal formation time

Mean values for daily enamel cross striation spacing in inner, middle and outer cuspal regions of the two fragments of FS#BC-nn were 4.32 μm, 5.29 μm, and 5.19 μm, respectively (see descriptive statistics in Table 4). Thus, there is a slight gradient of increasing rates of daily enamel formation from inner to outer cuspal enamel. The grand mean of these three cuspal means is 4.93 μm, which was rounded to 5 μm. Thus, the 1100 μm and 1200 μm of cuspal enamel in the two sections was estimated respectively to have taken 1100/5 = 220 days and 1200/5 = 240 days to form.

Following this general survey of cross striation measurements, a zone of enamel 200 μm thick from the EDJ was defined from the cusp to the cervix in both sections of the enamel fragments (FS#BC-nn). While there was a gradient of increasing enamel formation rate from the EDJ to the outer enamel, there was no cuspal-cervical gradient

Table 3
3D-based relative enamel thickness index (3D RET) in extant and fossil hominoids (decreasing values). Sample size is reported in parentheses near each taxon.
Tableau 3
Indice 3D d'épaisseur relative de l'émail (3D RET) chez des hominoïdes actuels et fossiles (valeurs décroissantes). La taille de l'échantillon est indiquée entre parenthèses près de chaque taxon.

Taxon	LM1	LM2	LM3	Mean	Category[l]
Ouranopithecus macedoniensis (1)[a]	28.5			28.5	Thick
Paranthropus robustus (4)[b]	25.0	20.9		24.0	
Range	18.6–32.1				
Homo sapiens (54)[a,c,m]	17.0	20.1	21.8	19.7	
Range	14.5–22.4	12.6–40.7	17.9–27.8		
Homo erectus (Asia) (7)[d,e]		21.4	18.0	21.7	
Range		19.0–23.6			
Gigantopithecus blacki (3)[f]				18.7	
Range					
Homo heidelbergensis (N Africa) (2)[g]		15.0	20.3	17.7	
Range					
Australopithecus africanus (7)[b]	20.6	15.7	15.5	17.0	Intermed-thick
Range	15.0–26.1	14.7–16.7	12.1–19.3		
Neanderthals (48)[e,h,i,j,m]	16.0	14.9	16.6	16.3	
Range	11.8–24.0	11.9–25.5	11.0–22.3		
Oreopithecus bambolii (3)[m]	14.2	16.4	16.2	15.6	
Homo erectus/ergaster (E Africa) (1)[k]	14.7			14.7	
Pongo pygmaeus (8)[c,m]	12.6	15.5	15.2	14.4	Intermed-thin
Range	11.7–13.3	12.8–19.0			
Pan troglodytes (22)[a,c]	12.0	11.6	12.4	12.0	
Range	9.3–16.4	9.6–12.8	9.0–14.7		
Gorilla gorilla (9)[a,c]	9.2	9.9		9.5	Thin
Range	7.1–10.5	8.1–11.7			

[a] Macchiarelli et al. (2009).
[b] Olejniczak et al. (2008c).
[c] Olejniczak et al. (2008d).
[d] Zanolli (2014).
[e] Macchiarelli et al. (2013).
[f] Kono et al. (2014).
[g] Zanolli and Mazurier (2013).
[h] Olejniczak et al. (2008a).
[i] Kupczik and Hublin (2010).
[j] NESPOS Database (2014).
[k] Zanolli et al. (2014).
[l] Following Martin (1985).
[m] This study.

within this inner zone close to the EDJ. The range of cross striation spacings did not change in this zone between the cusp and the cervix. The mean value of 26 measurements of cross striation spacing made within this zone between the cusp and cervix was 3.9 μm (Table 4). Thus, on average, any 200 μm thickness of enamel from the EDJ in these two *Oreopithecus* sections took 200/3.9 = 51 days to form (compared with mean values of 57 days in the *Pan* M2 sections and 62 days in the *Gorilla* M2 sections; see Dean, 1998). This calculation was then used to estimate total enamel formation times and enamel extension rates in these two sections following Dean (2009, 2010) and Guatelli-Steinberg et al. (2012).

4.4. Crown formation times

Following methods described previously (Dean, 2009, 2010; Guatelli-Steinberg et al., 2012), a measurement of 200 μm along a prism length (51 days formation time) was made from the EDJ tip in the cusp at the dentine horn. From this point an accentuated marking, or stria of Retzius, was identified and tracked obliquely back to intersect the EDJ further along from the dentine horn. The distance along the EDJ between the start-point at the dentine horn and the end-point further along the EDJ represents the length of EDJ formed in the same time it takes to form a 200 μm thickness of enamel (51 days). This represents the enamel extension rate that can be expressed in μm/day (see Section 4.5 below). This procedure was repeated from the cusp tip to the enamel cervix and each 51-day prism length cumulated to give the total enamel formation time. In both fragments there were 14 complete 51-day prism lengths so the total enamel formation time was 714 days in each fragment.

Crown formation time is equal to the sum of lateral enamel formation time and cuspal enamel formation time. The sum of cuspal enamel formation times (calculated in Section 4.3 above) and lateral enamel formation times in each of the enamel fragments (220 + 494 = 714 days) and (240 + 474 = 714 days) gives identical crown formation times of 1.96 years. However, the fragments are of unequal length along the EDJ from the cusp to the cervix. One fragment measures 7316 μm and the other 8230 μm.

Each section contained prominent accentuated lines within the enamel with an identical pattern in their relative

Table 4
Comparison of daily enamel formation rates in *Pan troglodytes*, *Gorilla gorilla* and *Oreopithecus bambolii*. When available, the range and/or standard deviation are indicated between parentheses. *n* is the number of measurements.
Tableau 4
Comparaison des taux de formation par jour de l'émail chez *Pan troglodytes*, *Gorilla gorilla* et *Oreopithecus bambolii*. Lorsque disponible, l'intervalle de variation et/ou l'écart-type sont indiqués entre parenthèses. *n* représente le nombre de mesures.

		Oreopithecus bambolii		*Pan troglodytes*		*Gorilla gorilla*
Inner cuspal						
Smith et al. (2007)	Molar average			*n* = 75	3.62 (2.78–4.72/± 0.42)	
Kelley et al. (2001)	M1, M2			*n* = 2	3.36, 3.57	
This study	Enamel Fragments	*n* = 22	4.32 (2.90–5.30/± 0.61)			
Beynon et al. (1991)	Molar average			*n* = 4	3.10 (± 0.30)	*n* = 5	3.20 (± 0.20)
This study	M2					*n* = 61	3.25 (2.48–4.07/± 0.32)
Middle cuspal						
Smith et al. (2007)	Molar average			*n* = 75	4.23 (3.01–5.38/± 0.50)	
Kelley et al. (2001)	M1, M2			*n* = 2	4.23, 4.18	
This study	Molar average	*n* = 13	5.29 (4.40–6.00/± 0.55)			
Beynon et al. (1991)	Molar average			*n* = 1	4.40	*n* = 5	5.20 (± 0.50)
Outer cuspal						
Smith et al. (2007)	Molar average			*n* = 75	4.60 (3.64–5.77/± 0.51)	
Kelley et al. (2001)	M1, M2			*n* = 2	4.67, 4.58	
This study	Enamel fragments	*n* = 20	5.19 (4.50–6.29/± 0.50)			
Beynon et al. (1991)	Molar average			*n* = 2	5.00 (± 0.50)	*n* = 5	6.10 (± 0.30)
Outer lateral						
Kelley et al. (2001)	M1, M2			*n* = 2	4.69, 4.19	
This study	M2	*n* = 5	5.18 (4.70–5.60/± 0.20)			
Beynon et al. (1991)	Molar average			*n* = 1	4.10	*n* = 5	6.10 (± 0.30)
Cervical enamel						
This study	M2	*n* = 13	3.94 (3.20–4.89/± 0.45)			
Beynon et al. (1991)	Molar average			*n* = 4	3.90 (± 0.30)	*n* = 5	3.80 (± 0.45)
All inner cross striations 0–00 μm from EDJ						
This study	Enamel fragments	*n* = 26	3.86 (2.90–5.20/± 0.56)			
This study	Molar average			*n* = 14	3.51 (3.28–4.08/± 0.24)	
This study	M2					*n* = 101	3.25 (2.34–4.13/± 0.35)

spacing (a white and a black arrow in Fig. 3A and B denote two accentuated lines). This makes it highly likely that both fragments belonged to the same tooth and may well represent the buccal or lingual aspects of a lower molar (or less likely, a premolar). Given this, it is perhaps not surprising that the enamel formation time estimate for each is the same. However, the taller enamel fragment has the first of these shared accentuated lines 230 μm further away from the EDJ in the cusp than observed in the shorter enamel fragment, suggesting ~ 46 days (i.e., 230/5 = 46 days) extra enamel formation in the former. It follows that this cusp is likely to have initiated earlier and to be staggered in its formation time with respect to the shorter fragment. Since enamel formation times are estimated to be equal in both fragments, the last-formed enamel may be in the cervix of the shorter fragment, ~ 6–7 weeks after it completed in the taller fragment. If this is the case, the total time taken to form enamel in this tooth would have been 2.08 years.

In summary, crown formation time in these enamel fragments (FS#BC-nn) was close to 2 years. If total enamel formation time was 714 days in each enamel fragment, then this minus the cuspal formation times (220 and 240 days, respectively) leaves 494 and 474 days to form the lateral enamel of each enamel fragment. With either

Table 5
Summary of the molar cusp formation times in *Oreopithecus* (crown fragments FS#BC-nn) compared with those of *Pan troglodytes*. *n* is *Pan* sample size.
Tableau 5
Temps de formation des cuspides des molaires chez *Oreopithecus* (fragments de couronne FS#BC-nn), comparés à ceux de *Pan troglodytes*. *n* représente la taille de l'échantillon de *Pan*.

	Oreopithecus	*Pan*
M1 protoconid	1.96	(*n* = 14) 2.30 (1.78–2.65)
M1 protoconid*		(*n* = 5) 2.17 (2.00–2.61)
M1 metaconid		(*n* = 7) 1.60 (1.41–1.87)
M1 metaconid*		(*n* = 5) 1.73 (1.65–1.87)
M2 protoconid	1.96	(*n* = 10) 2.38 (1.72–3.20)
M2 protoconid*		(*n* = 4) 2.69 (2.20–2.96)
M2 metaconid*	1.96	(*n* = 5) 2.33 (1.95–2.98)
M3 protoconid		(*n* = 10) 2.80 (2.19–3.34)
M3 protoconid*		(*n* = 1) 2.74
M3 metaconid*	1.96	(*n* = 2) 2.25 (1.91–2.60)

Data marked * are from (Smith et al. (2007): Table 6; originally cited in days).

5 or 6 days between striae of Retzius and perikymata in *Oreopithecus*, the expectation is that M2s would express between 80 and 100 perikymata between the cusp tip and cervix. This is explored further in Section 4.6 below.

A summary of crown (cusp-specific) enamel formation times in *Oreopithecus* compared with those of *Pan* appears in Table 5. The data for *Oreopithecus* are entered against each cusp for *Pan* where the range for almost all cusps on all molars would include our estimate for *Oreopithecus* of 1.96 years.

4.5. Enamel extension rates

Enamel extension rates in the two *Oreopithecus* ground sections (FS#BC-nn) were calculated for each 51-day increment of time beginning with crown initiation in the cusp tip at the dentine horn. In sequence from the dentine horn, these were initially 32, 14, 15 and 10 μm per day in one cusp and 26, 26, 15, 13, and 10 μm per day in the slightly taller fragment. At the enamel cervix extension rates were 5.5 μm per day in one section and 6.1 μm per day in the other. It was also possible to estimate enamel extension rates in the last part of the cervix of the LM2 belonging to IGF4883 V. Here daily enamel formation rates were slightly slower than in the other two sections (average 3.6 μm/day), so that each 200 μm thickness of enamel took 55.5 days and not 51 days to form. Cervical extension rates were measured twice in succession, 5.1 and 5.3 μm/day, and correspond well to the cervical enamel extension rates in the two enamel fragments.

A summary of maximum extension rates calculated in the buccal cusp tips of molar teeth for several taxa appears in Table 6.

4.6. Perikymata counts, periodicities and lateral enamel formation times

The buccal aspect of the LI2 FS#BC-23 (Fig. 2) was worn at the occlusal edge, but expressed in excess of 120 well-preserved perikymata from the cervix. The buccal aspect of the UC of IGF4332 is fractured at the cusp tip, but it expressed in excess of 140 perikymata that also are well-preserved from the cervix. On the same maxillary specimen, only incomplete counts on the lingual aspects of the UP4 (> 75), UM1 (> 75), and UM2 (> 85) were possible. Near-complete counts were possible on the buccal aspects of the well-preserved LP4 FS#Q16-64 (> 96), and LM2 FS#Q16-59 (> 75) (Fig. 2).

The two sections of the enamel fragments FS#BC-nn contained > 90 and > 80 long-period striae of Retzius, respectively. In each fragment at least 1 mm of enamel was worn away at the cusp tip that might have contained ~ 10, or more, extra perikymata. Regions of the lateral enamel show locations where 5 daily increments are visible between long-period striae of Retzius. This is not inconsistent with the estimated number of striae within these sections (Fig. 5) taking 494 days and 474 days, respectively, to form and suggests that we are observing a degree of internal consistency within the enamel microstructure of these *Oreopithecus* enamel fragments.

The section of the LM2 of IGF4883 V cervical enamel, on the other hand, showed clear daily cross striations ~ 3.6 μm apart on average but with regions slightly greater or smaller than this. Striae of Retzius were spaced ~ 18–20 μm apart and in places 6 increments were visible between adjacent striae (Fig. 5). Taking the evidence from both individuals studied here, a periodicity of 5 or 6 days between striae of Retzius seems likely in *Oreopithecus*. The number of striae counted in the two enamel fragments is comparable with the number of perikymata counted in the other *Oreopithecus* M2s (and P4s) reported above and exceeds the number observed in the UM1 of IGF4332. They support the diagnosis of each fragment belonging to an M2 rather than an M1 and their morphology, with a thick occlusal portion, favours them being M2 fragments rather than P4 fragments.

4.7. Growth in tooth height in Oreopithecus and Pan

Fig. 6 shows increase in tooth length along the EDJ continuing along the CDJ (cemento-dentine junction in the root) against tooth formation time. The data for each *Oreopithecus* enamel fragment (FS#BC-nn) are treated separately. The data for the M2 root growth of IGF4883 V have been added to that of the two crown fragments to produce a combined profile of crown and root growth for each fragment. When the data for *Oreopithecus* are plotted with the *Pan* M1 sample (Fig. 6A), they fall just beyond those teeth that achieve the greatest heights in the shortest times; however, when they are plotted with the *Pan* M2 sample (Fig. 6B), they lie well beyond the range observed for *Pan*.

5. Discussion

5.1. Tooth morphostructure

Our 3D virtual investigation revealed that the high and complex occlusal topography of the *Oreopithecus* molars is not only found externally (Butler and Mills, 1959), but is also reflected internally, where the dentine horns are particularly elevated and acute, linked by sharp ridges and accessory features (Zanolli et al., 2010). This unique morphology differs from the lower, more squat cusps

Table 6
Maximum molar cuspal enamel extension rates in extant and fossil catarrhine primates (decreasing values).
Tableau 6
Taux d'extension maximal de l'émail des cuspides des molaires chez des primates catarrhiniens actuels et fossiles (valeurs décroissantes).

Taxon	Tooth	*n*	Mean	SD	Range
Gorilla gorilla[a,b]	M1	6	39.6	13.4	23.7–52.5
	M2	5	44.9	3.2	42.8–50.2
	M3	1	49.9		
Neanderthals[b,c,d]	M1	1	34.7		
Victoriapithecus macinnesi[b,e]	M2	2	30.3		24.8–35.9
Oreopithecus bambolii[i]	**M2**	**2**	**29.3**		**32.1–26.5**
Homo sapiens[a,b]	M1	15	26.7	4.5	17.1–36.7
	M2	8	24.2	5.6	16.4–37.9
	M3	6	24.4	7.4	15.2–30.9
Proconsul nyanzae[b,f]	M1	1	31.7		
	M2	1	28.7		
Hispanopithecus laietanus[b,g]	M1	1	29.1		
	M2	1	22.1		
Gigantopithecus blacki[b,h]	M3	1	26.1		
Pan troglodytes[a]	M1	10	28.0	4.5	21.5–36.3
	M2	10	20.6	6.1	13.3–29.6
	M3	10	21.7	4.4	14.4–28.1
Australopithecus anamensis[a,b]	M1	1	17.6		

[a] Dean (2010).
[b] Guatelli-Steinberg et al. (2012).
[c] Macchiarelli et al. (2006).
[d] Dean (2009).
[e] Dean and Leakey (2004).
[f] Beynon et al. (1998).
[g] Dean and Kelley (2012).
[h] Dean and Schrenk (2003).
[i] This study.

and dentine horns enclosing a sub-concave occlusal basin commonly seen in fossil and extant hominoid molars, such as *Ouranopithecus* (Macchiarelli et al., 2009), *Paranthropus* and *Australopithecus* (Skinner et al., 2008a), *Homo* (Macchiarelli et al., 2006; Skinner et al., 2008b; Zanolli, 2014; Zanolli and Mazurier, 2013), and in the living great apes (Skinner et al., 2008b, 2010).

Assuming that *Oreopithecus* is closely related to the dryopithecines (Harrison and Rook, 1997; Moyà-Solà and Köhler, 1997), which almost invariably exhibit a low to only moderately elevated external crown topography (Alba et al., 2013; Begun, 2002), its tall occlusal reliefs could represent an autapomorphic feature developed under conditions of insular isolation. On the other hand, tall cusps could also represent the retention of a primitive feature, as seen in basal hominoids (Begun, 2002). Ongoing systematic characterization of the inner structural morphology of the dryopithecine molar crowns promises to shed light on this relevant aspect (Fortuny et al., 2014).

Oreopithecus displays thicker molar enamel than *Pan* and *Gorilla* (for both RET and 3D RET), but slightly thinner than extant humans. Compared to other fossil hominoids, on average, *Oreopithecus* shows thicker enamel than the dryopithecines reported so far (Alba et al., 2013). Interestingly, megadont fossil hominoids, such as *Ouranopithecus*, *Paranthropus*, *Australopithecus* and *Gigantopithecus*, show the relatively and absolutely thickest enamel, suggesting an allometric trend.

Variations in tooth enamel thickness result from a complex interplay between ecology and phylogeny (Horvath et al., 2014; Pampush et al., 2013; Smith et al., 2012). Traditionally used to infer durophagy in fossil primate taxa, it is now considered as intimately related to dietary abrasiveness and selectively responsive to lifetime dental wear resistance (Pampush et al., 2013). Because of its elevated cusps and sub-bilophodont molar pattern, *Oreopithecus* has been commonly regarded as a specialized leaf eater (e.g., Begun, 2007; Kay and Ungar, 1997; Szalay and Delson, 1979; but see Moyà-Solà and Köhler, 1997). However, stable isotopic analyses ($\delta^{18}O$, $\delta^{13}C$) suggest that, compared to modern chimpanzees or *Sivapithecus*, *Oreopithecus* exploited a wider range of habitats and food items (Nelson and Rook, 2008; Rook and Nelson, 2009). This is supported by microwear analyses that suggest a closer fit with *Papio ursinus* (DeMiguel et al., 2014; L'Engle Williams, 2013; Smith and Williams, 2010; Ungar, 1996). Accordingly, similarly to the variation in molar enamel thickness seen in macaques (Kato et al., 2014), the intermediate-thick (Martin, 1985) enamel of *Oreopithecus* could reflect wider dietary diversity implying the interaction with a greater range of food material properties than previously thought.

5.2. Crown heights, enamel thickness and enamel formation

High extension rates in the first-formed cuspal enamel play a large role in determining final cusp height and tooth height (Dean, 2009; Guatelli-Steinberg et al., 2012). Thereafter, a combination of extension rates and time spent forming enamel contribute to final crown height. Tall cusps and overall crown height (relatively higher in *Oreopithecus* than in *Pan* and *Gorilla*) are achieved with

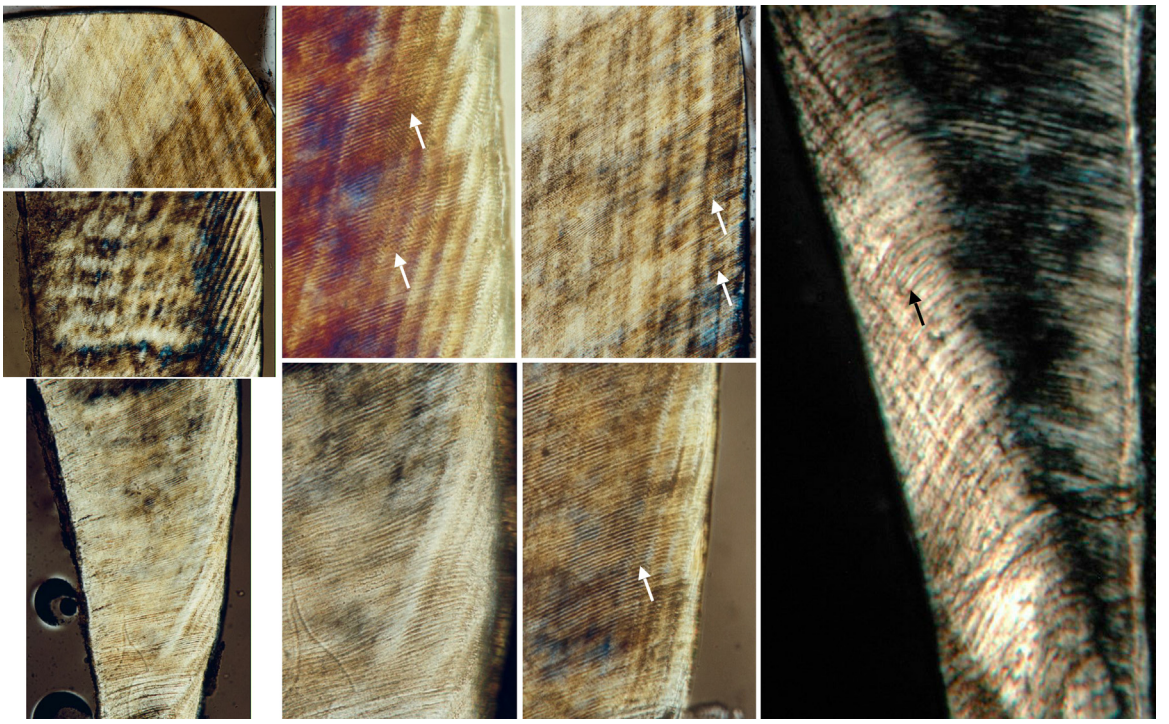

Fig. 5. (Color online.) *Oreopithecus bambolii*. Selected high-power images of the histological sections showing well discernible striae in various regions of the crown (inner and outer enamel). The white arrows indicate areas where 5 cross striations are visible between adjacent striae in the two enamel fragments FS#BC-nn, while the black arrow highlights a portion of the cervical enamel of the LM2 IGF4883V with 6 increments visible between adjacent striae.
Fig. 5. (Couleur en ligne.) *Oreopithecus bambolii*. Sélection d'images de sections histologiques à haute résolution montrant les stries bien discernables dans plusieurs parties de la couronne (émail interne et externe). Les flèches blanches indiquent les zones où 5 striations croisées sont visibles entre des stries adjacentes dans les deux fragments d'émail FS#BC-nn, tandis que les flèches noires montrent une portion de l'émail cervical de la LM2 IGF4883V avec 6 striations visibles entre des stries adjacentes.

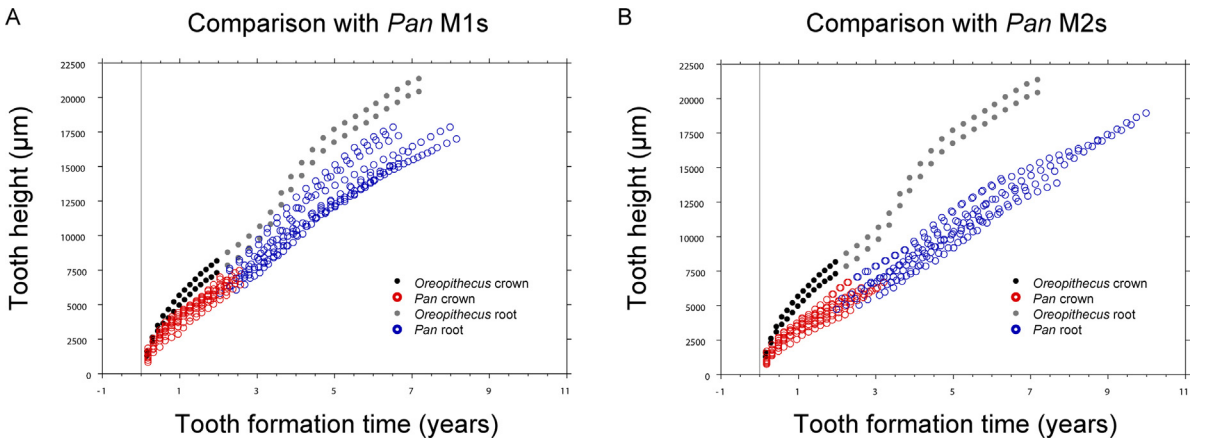

Fig. 6. (Color online.) Plots of increasing tooth height (µm) against crown (enamel fragments FS#BC-nn) and root (LM2 IGF4883V) formation time (years) in *Oreopithecus* (black crown and grey root dots) and *Pan troglodytes* (red crown and blue root open circles) first molar (A) and second molar (B).
Fig. 6. (Couleur en ligne.) Augmentation de la hauteur de la couronne (µm) en fonction du temps de formation (en années) de la couronne (fragments d'émail FS#BC-nn) et de la racine (LM2 IGF4883 V) de la première (A) et de la seconde molaire (B) chez *Oreopithecus* (points noirs pour la couronne et gris pour la racine) et *Pan troglodytes* (cercles rouges pour la couronne et bleus pour la racine).

fast initial cuspal extension rates that are maintained into crown formation, as they appear also to be in the Miocene cercopithecoid *Victoriapithecus macinnesi* (Fig. 7; Dean and Leakey, 2004). The dryopithecine *Hispanopithecus laietanus* (Alba et al., 2012; Dean and Kelley, 2012; Kelley et al., 2001), which is more similar to extant and fossil hominins and pongines than to *Oreopithecus* in molar occlusal morphology, has a slower initial crown growth trajectory but continues growing in height for a long period of time.

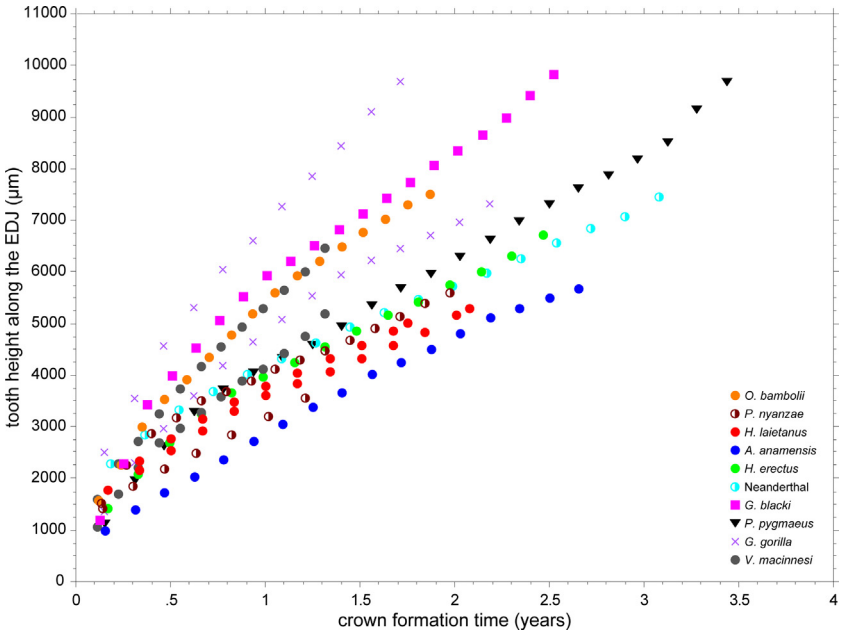

Fig. 7. (Color online.) Plot of increasing tooth height along the EDJ (µm) against crown formation time (years) in *Oreopithecus* (orange filled circles) and a number of extant and fossil catarrhine primates.
Fig. 7. (Couleur en ligne.) Augmentation de la hauteur de la couronne le long de l'EDJ (µm) en fonction du temps de formation de la couronne (en années) chez *Oreopithecus* (disques orange) et un certain nombre de primates catarrhiniens actuels et fossiles.

Table 6 demonstrates how variable the initial maximum cuspal extension rates are in samples of extant taxa. It also evidences how maximum cuspal extension rates observed in *Oreopithecus* fall within the gorilla, chimpanzee and modern human ranges, but along with those of *Victoriapithecus macinnesi* tend towards the higher values for M2s than fossil hominids with lower more squat crown morphologies.

Oreopithecus cuspal enamel overall grew at a fast daily rate (Table 7) and the three molars from Fiume Santo analysed here approach the relative enamel thickness values reported for *Afropithecus turkanensis, Sivapithecus parvada* and *Australopithecus africanus* (Mahoney et al., 2007; Olejniczak et al., 2008c; Smith et al., 2003). The overall faster daily rates, especially in the inner cuspal enamel, may be part of the process of achieving this degree of thickness in a given crown formation time.

In the Old World monkey *Victoriapithecus macinnesi* (Dean and Leakey, 2004), there was a near constant secretion rate of 6 µm/day in the M2 cuspal enamel, which is consistently higher than in Miocene apes or thick-enamelled hominins. It is possible this is the primitive condition we might expect for a stem hominoid, but this is not the case in *Oreopithecus*, where a slight gradient exists from ~4 to 5 µm/day (Table 7). In *Proconsul nyanzae*, the cuspal enamel gradient ranged from ~4 to 6 µm/day, with inner rates staying slower for a longer time (Beynon et al., 1998). Thus, the gradient in *Proconsul nyanzae* was more pronounced than in *Oreopithecus.*

Based on our evidence, it seems there is no simple relationship between the thickness of cuspal enamel and the gradients of daily formation rates within them (see Table 7).

5.3. The periodicity of striae of Retzius (perikymata) and crown formation times

Very few of the 75 chimpanzees studied by Smith et al. (2007) had periodicities as low as 5 ~ days. The 5-day periodicity in the two of the three *Oreopithecus* enamel fragments resembles, therefore, the modal value in macaque monkeys, and that occasionally seen in gibbons (Beynon et al., 1998; Dirks, 1998). The 5- and 6-day periodicities in the two *Oreopithecus* individuals reported here may turn out to be close to the modal periodicity in *Oreopithecus*, in which case it might best be explained with respect to what we know of its body size, where males were perhaps the size of a female chimpanzee, or slightly smaller, and females the size of a male baboon (Jungers, 1987). However, the nature and strength of the relationship between long-period stria periodicity and body size remain unclear.

The comparison with the data available for *Pan* (Table 5) would suggest the *Oreopithecus* fragments FS#BC-nn have greater formation times than *Pan* M1 metaconids. But the small sample of M1 or M2 protoconid formation times in *Pan* both encompasses the time to form these fragments. Even M3 metaconid formation times in *Pan* encompass 2 years, and M3 protoconid formation times are only a little more than 2 years at the low end of their range (Table 5). One fragment of FS#BC-nn has the typical concave EDJ of lower buccal or upper palatal cusp EDJs but the other does not (Fig. 3A and 3B). It is possible that the taller later initiating enamel fragment is a lower lingual or upper buccal fragment from the contralateral side of the shorter fragment. If this is the case then, unlike *Pan* M1s but similar

Table 7
Gradients of cuspal enamel formation in extant and fossil catarrhine primates (increasing % values).
Tableau 7
Gradients de formation de l'émail des cuspides chez des primates catarrhiniens actuels et fossiles (valeurs croissantes en %).

	Cuspal inner rate (μm/day)	Cuspal outer rate (μm/day)	Percentage increase (%)
Ouranopithecus macedoniensis[a]	4.15	4.30	3.60
Victoriapithecus macinnesi[b]	5.65	6.50	15.00
Sivapithecus indicus[c]	4.38	5.15	17.60
Oreopithecus bambolii[m]	4.32	5.19	20.10
Afropithecus turkanensis[d]	3.97	4.85	22.20
Sivapithecus parvada[c]	4.48	5.50	22.80
Proconsul nyanzae[e]	4.40	5.50	25.00
Proconsul heseloni[e]	4.40	5.50	25.00
Pan troglodytes[f]	3.62	4.62	27.60
Australopithecus anamensis[g]	4.17	5.47	31.20
Homo habilis[g]	3.68	5.22	41.80
Gigantopithecus blacki[h]	4.10	6.00	46.30
Australopithecus africanus[g]	4.18	6.62	58.40
Pongo pygmaeus[i]	3.27	5.20	59.00
Gorilla gorilla[i]	3.37	5.47	62.30
Hispanopithecus laietanus[j]	3.25	5.50	69.20
Homo erectus[g]	3.05	5.19	70.20
Neanderthal (La Chaise)[k]	2.93	5.00	70.60
Paranthropus robustus[g]	4.16	7.25	74.30
Australopithecus afarensis[g]	3.31	5.84	76.40
Homo rudolfensis[g]	3.01	5.38	78.70
Neanderthal (Tabun)[k]	3.16	5.81	84.10
Homo sapiens (average)[g]	2.80	5.20	85.70
Paranthropus aethiopicus[g]	3.50	6.53	86.60
Lufengpithecus hudienensis[l]	3.00	5.60	86.70
Paranthropus boisei[g]	2.94	7.15	143.20

[a] Smith et al. (2004).
[b] Dean and Leakey (2004).
[c] Mahoney et al. (2007).
[d] Smith et al. (2003).
[e] Beynon et al. (1998).
[f] Smith et al. (2007).
[g] Lacruz et al. (2008).
[h] Dean and Schrenk (2003).
[i] Dean (1998).
[j] Dean and Kelley (2012).
[k] Macchiarelli et al. (2006).
[l] Schwartz et al. (2003).
[m] This study.

to *Pan* M2s, both aspects of this *Oreopithecus* tooth would have had similar total enamel formation times.

The evidence based on the shared internal pattern of accentuated markings, the thick-enamelled occlusal projection in one fragment, as well as identical enamel formation times and the surface perikymata counts within the *Oreopithecus* sample itself, support these fragments very likely coming from the same M2 crown (but not completely excluding a P4 attribution due to its similar formation times with the M2).

In *Oreopithecus*, the crown formation times of the two possible M2s fragments were ~1.96 years, close to those reported for *Proconsul nyanzae* (~2 years; Beynon et al., 1998).

5.4. Comparative dental development in Oreopithecus

Values for most of the variables described here for *Oreopithecus* fit well within what is known for *Pan*. Those at the upper limits of variation known for *Pan* (the high M2 cuspal extension rates in the crown) can be considered as part of an adaptation to grow a tall crown. The faster rates of enamel formation are harder to interpret, but might simply be an adaptation to grow thick enamel in a short period of time. By way of example, faster rates of enamel formation in *Paranthropus boisei* than in *Pan troglodytes* do not appear to be linked with any obvious differences in their crown formation times (Lacruz et al., 2008), but they do contribute to crowns with thick enamel being able to complete their formation within a similar time to those of *Pan*. Thick enamel in *Ouranopithecus macedoniensis* (Macchiarelli et al., 2009; Smith et al., 2004) appears to have formed with a minimal gradient of enamel formation from the EDJ to the surface enamel (Table 7), and so no clear link between enamel gradients and enamel thickness appear to exist among hominoids. These new data for *Oreopithecus* serve to emphasise that thick enamel may form in many ways.

A larger sample of *Oreopithecus* molars would demonstrate if faster enamel formation rates are actually associated with shorter than average crown formation times than in *Pan*. The non-destructive analytical method

described here (See Section 4.3) would facilitate studies of larger samples of individuals than in this study and might resolve the question of whether the mean total crown formation times for a sample of *Oreopithecus* molars were actually less than in *Pan*. It is not presently possible to know, however, whether a single *Oreopithecus* specimen is representative of the mean of this taxon. The crown formation time for the individual used in this study (~2 years) falls within the ranges known for *Pan* M1 and M2 crown formation. However, in addition to individual crown formation times, the initiation times of tooth mineralisation and the degree to which M1, M2 and M3 crown formation periods overlap with one another, which is quite variable in *Pan* and *Pongo* (Smith et al., 2007; Winkler et al., 1991), together best reflect the overall duration of dental development (Dean, 2010). Previously, early molar initiation times were shown to play a key role in the accelerated dental development of *Anapithecus hernyaki* (Nargolwalla et al., 2005). Information made available from this study concerning the timing of individual molar tooth formation in *Oreopithecus* would be more informative if it were possible to determine both the degree of overlap in molar formation and the initiation times of individual molar crowns.

Acknowledgements

We congratulate the initiative of this Palevol thematic issue promoted by M. Laurin and J. Cubo and sincerely thank both co-editors for their kind invitation to contribute a paper. The present version of our paper greatly benefited from the critical comments and suggestions from two reviewers. For access to *Oreopithecus* specimens under their care, we are grateful to L. Trebini (Soprintendenza per i Beni Archeologici per le Province di Sassari e Nuoro), E. Cioppi (Museo di Storia Naturale, Università di Firenze), B. Engesser and L. Costeur (Basel Naturhistorisches Museum). Paleontological fieldwork at Fiume Santo has been carried out under an agreement between the Soprintendenza per i Beni Archeologici per le Province di Sassari e Nuoro and the Earth Sciences Department of the University of Florence. Field research has been possible thanks to financial support from the National Geographic Society (grant #7484-03 to L.R.), the RHOI program at University of Berkeley (project NSF-BCS-0321893), and the logistic support of ENDESA Italia. For continuous support during fieldwork at Fiume Santo, L.R. thanks the team of the Paleontology Section within the local office of the Soprintendenza Archeologica (L. Trebini, N. Tuveri, and M. Arca), as well as the precious collaboration offered by M. Delfino, G. Gallai, and L. Abbazzi. A.M. and R.M. acknowledge L. de Bonis for having granted access to the *Ouranopithecus* dental material used for comparison. The acquisitions at the ESRF Grenoble have been realized by A.M., L.B. and R.M. thanks the valuable support provided by A. Bravin, C. Nemoz and P. Tafforeau. We thank D. Alba and J. Kelley for the very useful comments provided to the first version of our study. L.B., L.R. and R.M. do not forget their friend M. Rossi, physicist at the Univ. of Bologna, who first revealed by microtomography the inner structural morphology of the *Oreopithecus* teeth.

References

Abbazzi, L., Delfino, M., Gallai, G., Trebini, L., Rook, L., 2008. New data on the vertebrate assemblage of Fiume Santo (North-West Sardinia, Italy), and overview on the Late Miocene Tusco-Sardinian palaeobioprovince. Palaeontology 51, 425–451.

Alba, D.M., 2012. Fossil Apes from the Vallès-Penedès Basin. Evol. Anthropol. 21, 254–269.

Alba, D.M., Casanovas-Vilar, I., Almécija, S., Robles, J.M., Arias-Martorell, J., Moyà-Solà, S., 2012. New dental remains of *Hispanopithecus laietanus* (Primates: Hominidae) from Can Llobateres 1 and the taxonomy of Late Miocene hominoids from the Vallès-Penedès Basin (NE Iberian Peninsula). J. Hum. Evol. 63, 231–246.

Alba, D.M., Fortuny, J., Pérez de los Ríos, M., Zanolli, C., Almécija, S., Casanovas-Vilar, I., Robles, J.M., Moyà-Solà, S., 2013. New dental remains of *Anoiapithecus* and the first appearance datum of hominoids in the Iberian Peninsula. J. Hum. Evol. 65, 573–584.

Alba, D.M., Moyà-Solà, S., Köhler, M., 2001a. Canine reduction in the Miocene hominoid *Oreopithecus bambolii*: behavioural and evolutionary implications. J. Hum. Evol. 40, 1–16.

Alba, D.M., Moyà-Solà, S., Köhler, M., Rook, L., 2001b. Heterochrony and the cranial anatomy of *Oreopithecus*: some cladistic fallacies and the significance of developmental constraints in phylogenetic analysis. In: de Bonis, L., Koufos, G.D., Andrews, P. (Eds.), Hominoid Evolution and Climatic Change in Europe, volume 2. Phylogeny of the Neogene Hominoid Primates of Eurasia. Cambridge University Press, Cambridge, pp. 284–315.

Andrews, P., Martin, L.B., 1991. Hominoid dietary evolution. Phil. Trans. R. Soc. London B 334, 199–209.

Begun, D.R., 2002. European hominoids. In: Hartwig, W.C. (Ed.), The Primate Fossil Record. Cambridge University Press, Cambridge, pp. 339–368.

Begun, D.R., 2007. Fossil record of Miocene hominoids. In: Henke, W., Tattersall, I. (Eds.), Handbook of Paleoanthropology. Springer, New York, pp. 921–977.

Benvenuti, M., Papini, M., Rook, L., 2001. Mammal biochronology, UBSU and paleoenvironment evolution in a post-collisional basin: evidence from the Late Miocene Baccinello-Cinigiano basin in southern Tuscany, Italy. Boll. Soc. Geol. It. 51, 97–118.

Beynon, A.D., Dean, M.C., Leakey, M.G., Reid, D.J., Walker, A., 1998. Comparative dental development and microstructure of *Proconsul* teeth from Rusinga Island, Kenya. J. Hum. Evol. 35, 163–209.

Beynon, A.D., Dean, M.C., Reid, D.J., 1991. Histological study on the chronology of the developing dentition in gorilla and orangutan. Am. J. Phys. Anthropol. 86, 189–203.

Butler, P.M., Mills, J.R.E., 1959. A contribution to the odontology of *Oreopithecus*. Bull. Brit. Mus. Nat. Hist. Geol. 4, 1–26.

Casanovas-Vilar, I., Alba, D.M., Garcés, M., Robles, J.M., Moyà-Solà, S., 2011b. Updated chronology for the Miocene hominoid radiation in western Eurasia. Proc. Natl. Acad. Sci. U S A 108, 5554–5559.

Casanovas-Vilar, I., Van Dam, J.A., Trebini, L., Rook, L., 2011a. The rodents from the Late Miocene *Oreopithecus*-bearing site of Fiume Santo (Sardinia, Italy). Geobios 44, 173–187.

Chaimanee, Y., Jolly, D., Benammi, M., Tafforeau, P., Duzer, D., Moussa, I., Jaeger, J.J., 2003. A Middle Miocene hominoid from Thailand and orangutan origins. Nature 422, 61–65.

Chaimanee, Y., Yamee, C., Tian, P., Khoawiset, K., Marandat, B., Tafforeau, P., Nemoz, C., Jaeger, J.J., 2006. *Khoratpithecus piriyai*, a Late Miocene hominoid of Thailand. Am. J. Phys. Anthropol. 131, 311–323.

Coleman, M.N., Colbert, M.W., 2007. Technical note: CT thresholding protocols for taking measurements on three-dimensional models. Am. J. Phys. Anthropol. 133, 723–725.

Cordy, J.M., Ginesu, S., 1994. Fiume Santo (Sassari, Sardaigne, Italie) : un nouveau gisement à Oréopithèque (Oreopithecidae, Primates, Mammalia). C.R. Acad. Sci., Paris, Ser. II 318, 697–703.

Corruccini, R.S., 1987. The dentinoenamel junction in primates. Intl. J. Primatol. 8, 99–114.

Dean, M.C., 1998. A comparative study of cross striation spacings in cuspal enamel and of four methods of estimating the time taken to grow molar cuspal enamel in *Pan*, *Pongo* and *Homo*. J. Hum. Evol. 35, 449–462.

Dean, M.C., 2009. Extension rates and growth in tooth height of modern human and fossil hominin canines and molars. In: Koppe, T., Meyer, G., Alt, K.W. (Eds.), Frontiers of Oral Biology: Interdisciplinary Dental Morphology. Karger, Basel, pp. 68–73.

Dean, M.C., 2010. Retrieving chronological age from dental remains of early fossil hominins to reconstruct human growth in the past. Phil. Trans. Royal Soc. B 365, 3397–3410.

Dean, M.C., Kelley, J., 2012. Comparative dental development in *Hispanopithecus laietanus* and *Pan troglodytes*. J. Hum. Evol. 62, 174–178.
Dean, M.C., Leakey, M.G., 2004. Enamel and dentine development and the life history profile of *Victoriapithecus macinnesi* from Maboko Island, Kenya. Ann. Anat. 186, 405–412.
Dean, M.C., Schrenk, F., 2003. Enamel thickness and development in a third permanent molar of *Gigantopithecus backi*. J. Hum. Evol. 45, 381–387.
Dean, M.C., Wood, B., 2003. A digital radiographic atlas of great apes skull and dentition. In: Bondioli, L., Macchiarelli, R. (Eds.), Digital Archives of Human Paleobiology. ADS Solutions, Milan (CD-ROM).
Delson, E., 1986. An anthropoid enigma: historical introduction to the study of *Oreopithecus bambolii*. J. Hum. Evol. 15, 523–531.
DeMiguel, D., Alba, D.M., Moyà-Solà, S., 2014. Dietary Specialization during the evolution of western Eurasian hominoids and the extinction of European great apes. PLoS One 9, e97442, http://dx.doi.org/10.1371/journal.pone.0097442.
Dirks, W., 1998. Histological reconstruction of dental development and age at death in a juvenile gibbon (*Hylobates lar*). J. Hum. Evol. 35, 411–425.
Fajardo, R.J., Ryan, T.M., Kappelman, J., 2002. Assessing the accuracy of high-resolution X-ray computed tomography of primate trabecular bone by comparisons with histological sections. Am. J. Phys. Anthropol. 118, 1–10.
Fortuny, J., Zanolli, C., Macchiarelli, R., Bernardini, F., Tuniz, C., Alba, D.M., 2014. Relative enamel thickness and enamel-dentine junction morphology in the Vallès-Penedès hominoids: a 3D approach based on X-ray micro-computed-tomography. Am. J. Phys. Anthropol. suppl. 58, 119–120 (abstract).
Gervais, P., 1872. Sur un singe fossile, d'espèce non encore décrite, qui a été découvert au Monte-Bamboli (Italie). C.R. Acad. Sci. Paris 74, 1217–1223.
Grine, F.E., 2005. Enamel thickness of deciduous and permanent molars in modern *Homo sapiens*. Am. J. Phys. Anthropol. 126, 14–31.
Guatelli-Steinberg, D., Floyd, B.A., Dean, M.C., Reid, D.J., 2012. Enamel extension rate patterns in modern human teeth: two approaches designed to establish an integrated context for fossil primates. J. Hum. Evol. 63, 475–486.
Güleç, E.S., Sevim, A., Pehlevan, C., Kaya, F., 2007. A new great ape from the Late Miocene of Turkey. Anthropol. Sci. 115, 153–158.
Harrison, T., Rook, L., 1997. Enigmatic anthropoid or misunderstood ape? The phylogenetic status of *Oreopithecus bambolii* reconsidered. In: Begun, D.R., Ward, C.V., Rose, M.D. (Eds.), Function, Phylogeny, and Fossils. Miocene Hominoid Evolution and Adaptations. Plenum Press, New York, pp. 327–362.
Horvath, J.E., Ramachandran, G.L., Fedrigo, O., Nielsen, W.J., Babbitt, C.C., Clair, St., Pfefferle, E.M., Jernvall, L.W., Wray, J., Wall, G.A.C.E., 2014. Genetic comparisons yield insight into the evolution of enamel thickness during human evolution. J. Hum. Evol. 73, 75–87.
Jungers, W.L., 1987. Body size and morphometric affinities of the appendicular skeleton in *Oreopithecus bambolii* (IGF 11778). J. Hum. Evol. 16, 445–456.
Kato, A., Tang, N., Borries, C., Papakyrikos, A.M., Hinde, K., Miller, E., Kunimatsu, Y., Hirasaki, E., Shimizu, D., Smith, T.M., 2014. Intra- and interspecific variation in macaque molar enamel thickness. Am. J. Phys. Anthropol. 155, 447–459.
Kay, R.F., Ungar, P.S., 1997. Dental evidence for diet in some Miocene catarrhines with comments on the effects of phylogeny on the interpretation of adaptation. In: Begun, D.R., Ward, C.V., Rose, M.D. (Eds.), Function, Phylogeny and Fossils: Miocene Hominoid Evolution and Adaptations. Plenum Publishing Co., New York, pp. 131–151.
Kelley, J., Dean, M.C., Reid, D.J., 2001. Molar growth in the Late Miocene hominoid *Dryopithecus laietanus*. In: Brook, A. (Ed.), 12th International Symposium on Dental Morphology. Sheffield Academic Press, Sheffield, pp. 123–134.
Köhler, M., Moyà-Solà, S., 1997. Ape-like or hominid-like? The positional behavior of *Oreopithecus bambolii* reconsidered. Proc. Natl. Acad. Sci. U S A 94, 11747–11750.
Köhler, M., Moyà-Solà, S., 2003. Understanding the enigmatic ape *Oreopithecus bambolii*. Cour. Forschung. Senckenberg 243, 111–123.
Kono, R.T., 2004. Molar enamel thickness and distribution patterns in extant great apes and humans: new insights based on a 3-dimensional whole crown perspective. Anthropol. Sci. 112, 121–146.
Kono, R.T., Zhang, Y., Jin, C., Takai, M., Suwa, G., 2014. A 3-dimensional assessment of molar enamel thickness and distribution pattern in *Gigantopithecus blacki*. Quat. Intl., http://dx.doi.org/10.1016/j.quaint.2014.02.012.
Kupczik, K., Hublin, J.J., 2010. Mandibular molar root morphology in Neanderthals and Late Pleistocene and recent *Homo sapiens*. J. Hum. Evol. 59, 525–541.
Lacruz, R.S., Dean, M.C., Ramirez Rozzi, F., Bromage, T.G., 2008. Megadontia, stria periodicity and patterns of enamel secretion in Plio-Pleistocene fossil hominins. J. Anat. 213, 148–158.
L'Engle Williams, F., 2013. Enamel microwear texture properties of IGF 11778 (*Oreopithecus bambolii*) from the Late Miocene of Baccinello, Italy. J. Anthropol. Sci. 91, 201–217.
Macchiarelli, R., Bayle, P., Bondioli, L., Mazurier, A., Zanolli, C., 2013. From outer to inner structural morphology in dental anthropology. The integration of the third dimension in the visualization and quantitative analysis of fossil remains. In: Scott, R.G., Irish, J.D. (Eds.), Anthropological Perspectives on Tooth Morphology: Genetics, Evolution, Variation. Cambridge University Press, Cambridge, pp. 250–277.
Macchiarelli, R., Bondioli, L., Debénath, A., Mazurier, A., Tournepiche, J.F., Birch, W., Dean, M.C., 2006. How Neanderthal molar teeth grew. Nature 444, 748–751.
Macchiarelli, R., Bondioli, L., Falk, D., Faupl, P., Illerhaus, B., Kullmer, O., Richter, W., Said, H., Sandrock, O., Schäfer, K., Urbanek, C., Viola, B.T., Weber, G.W., Seidler, H., 2004. Early Pliocene hominid tooth from Galili, Somali Region, Ethiopia. Coll. Antropol. 28, 65–76.
Macchiarelli, R., Bondioli, L., Mazurier, A., 2008. Virtual dentitions: touching the hidden evidence. In: Irish, J.D., Nelson, G.C. (Eds.), Technique and Application in Dental Anthropology. Cambridge University Press, Cambridge, pp. 426–448.
Macchiarelli, R., Mazurier, A., Illerhaus, B., Zanolli, C., 2009. *Ouranopithecus macedoniensis*: virtual reconstruction and 3D analysis of a juvenile mandibular dentition (RPl-82 and RPl-83). Geodiversitas 31, 851–863.
Macchiarelli, R., Mazurier, A., Volpato, V., 2007. L'apport des nouvelles technologies à l'étude des Néandertaliens. In: Vandermeersch, B., Maureille, B. (Eds.), Les Néandertaliens. Biologie et Cultures. Comité des Travaux Historiques et Scientifiques (CTHS), Paris, pp. 169–179.
Mahoney, P., Smith, T.M., Schwartz, G.T., Dean, M.C., Kelley, J., 2007. Molar crown formation in the Late Miocene Asian hominoids, *Sivapithecus pavarda* and *Sivapithecus indicus*. J. Hum. Evol. 53, 61–68.
Martin, L.B., 1985. Significance of enamel thickness in hominoid evolution. Nature 314, 260–263.
Mazurier, A., Volpato, V., Macchiarelli, R., 2006. Improved noninvasive microstructural analysis of fossil tissues by means of SR-microtomography. Appl. Phys. A Mat. Sc. Proc 83, 229–233.
Moyà-Solà, S., Köhler, M., 1997. The phylogenetic relationship of *Oreopithecus bambolii* Gervais, 1872. C.R. Acad. Sci. Paris, Ser. IIa 324, 141–148.
Nargolwalla, M.C., Begun, D.R., Dean, M.C., Reid, D.J., Kordos, L., 2005. Dental development and life history in *Anapithecus hernyaki*. J. Hum. Evol. 49, 99–122.
Nelson, S.V., Rook, L., 2008. Reconstructing *Oreopithecus*' paleoecology by means of stable isotopic analyses: preliminary data. Simp. Soc. Paleont. Ital., Siena, Accad. Fisiocritici, 139–140.
NESPOS Database, 2014. Neanderthal Studies Professional Online Service. http://www.nespos.org
Olejniczak, A.J., Gilbert, C.C., Martin, L.B., Smith, T.M., Ulhaas, L., Grine, F.E., 2007. Morphology of the enamel-dentine junction in sections of anthropoid primate maxillary molars. J. Hum. Evol. 53, 292–301.
Olejniczak, A.J., Martin, L., Ulhaas, L., 2004. Quantification of dentine shape in anthropoid primates. Ann. Anat. 186, 479–485.
Olejniczak, A.J., Smith, T.M., Feeney, R.N.M., Macchiarelli, R., Mazurier, A., Bondioli, L., Rosas, A., Fortea, J., de la Rasilla, M., Garcia-Tabernero, A., Radovcic, J., Skinner, M.M., Toussaint, M., Hublin, J.J., 2008a. Dental tissue proportions and enamel thickness in Neandertal and modern human molars. J. Hum. Evol. 55, 12–23.
Olejniczak, A.J., Smith, T.M., Skinner, M.M., Grine, F.E., Feeney, R.N.M., Thackeray, J.F., Hublin, J.J., 2008c. Three-dimensional molar enamel distribution and thickness in *Australopithecus* and *Paranthropus*. Biol. Lett. 4, 406–410.
Olejniczak, A.J., Smith, T.M., Wang, W., Potts, R., Ciochon, R., Kullmer, O., Schrenk, F., Hublin, J.J., 2008b. Molar enamel thickness and dentine horn height in *Gigantopithecus blacki*. Am. J. Phys. Anthropol. 135, 85–91.
Olejniczak, A.J., Tafforeau, P., Feeney, R.N.M., Martin, L.B., 2008d. Three-dimensional primate molar enamel thickness. J. Hum. Evol. 54, 187–195.
Pampush, J.D., Duque, A.C., Burrows, B.R., Daegling, D.J., Kenney, W.F., McGraw, W.S., 2013. Homoplasy and thick enamel in primates. J. Hum. Evol. 64, 216–224.
Rook, L., Bondioli, L., Köhler, M., Moyà-Solà, S., Macchiarelli, R., 1999. *Oreopithecus* was a bipedal ape after all: evidence from the iliac cancellous architecture. Proc. Natl. Acad. Sci. U S A 96, 8795–8799.

Rook, L., Gallai, G., Torre, D., 2006. Lands and endemic mammals in the Late Miocene of Italy: constraints for paleogeographic outlines of Tyrrhenian area. Palaeogeogr. Palaeoclimatol. Palaeoecol. 238, 263–269.
Rook, L., Harrison, T., Engesser, B., 1996. The taxonomic status and biochronological implications of new finds of *Oreopithecus* from Baccinello (Tuscany, Italy). J. Hum. Evol. 30, 3–27.
Rook, L., Nelson, S.V., 2009. Paleoecology of *Oreopithecus bambolii* faunas (Tuscany and Sardinia): stable isotopic analyses results. Acta Nat. Ateneo Parmense 45, 242 (abstract).
Rook, L., Oms, O., Benvenuti, M.G., Papini, M., 2011. Magnetostratigraphy of the Late Miocene Baccinello-Cinigiano basin (Tuscany, Italy) and the age of *Oreopithecus bambolii* faunal assemblages. Palaeogeogr. Palaeoclimatol. Palaeoecol. 305, 286–294.
Rossi, M., Casali, F., Romani, D., Bondioli, L., Macchiarelli, R., Rook, L., 2004. MicroCTscan in paleobiology: application to the study of dental tissues. Nucl. Instr. Meth. Phys. Res. B 213, 747–750.
Schneider, C.A., Rasband, W.S., Eliceiri, K.W., 2012. NIH Image to ImageJ: 25 years of image analysis. Nat. Meth. 9, 671–675.
Schwartz, G.T., Liu, W., Zheng, L., 2003. Preliminary investigation of dental microstructure in the Yuanmou hominoid, Yunnan Province, China. J. Hum. Evol. 44, 189–202.
Skinner, M.M., Evans, A., Smith, T.M., Jernvall, J., Tafforeau, P., Kupczik, K., Olejniczak, A.J., Rosas, A., Radovčić, J., Thackeray, J.F., Toussaint, M., Hublin, J.J., 2010. Brief communication: contributions of enamel-dentine junction shape and enamel deposition to primate molar crown complexity. Am. J. Phys. Anthropol. 142, 157–163.
Skinner, M.M., Gunz, P., Wood, B.A., Hublin, J.J., 2008a. Enamel-dentine junction (EDJ) morphology distinguishes the lower molars of *Australopithecus africanus* and *Paranthropus robustus*. J. Hum. Evol. 55, 979–988.
Skinner, M.M., Wood, B.A., Boesch, C., Olejniczak, A.J., Rosas, A., Smith, T.M., Hublin, J.J., 2008b. Dental trait expression at the enamel-dentine junction of lower molars in extant and fossil hominoids. J. Hum. Evol. 54, 173–186.
Smith, A.K., Williams, F.L., 2010. Assessing the dental microwear of *Oreopithecus* using low-magnification stereomicroscopy. Am. J. Phys. Anthropol. S50, 280–281 (abstract).
Smith, T.M., Bacon, A.M., Demeter, F., Kullmer, O., Nguyen, K.T., de Vos, J., Wei, W., Zermeno, J.P., Zhao, L., 2011. Dental tissue proportions in fossil orangutans from mainland Asia and Indonesia. Hum. Origins Res. 1, e1.
Smith, T.M., Martin, L.B., Leakey, M.G., 2003. Enamel thickness, microstructure and development in *Afropithecus turkanensis*. J. Hum. Evol. 44, 283–306.
Smith, T.M., Martin, L.B., Reid, D.J., de Bonis, L., Koufos, G.D., 2004. An examination of dental development in *Graecopithecus freybergi* (=*Ouranopithecus macedoniensis*). J. Hum. Evol. 46, 551–577.
Smith, T.M., Olejniczak, A.J., Kupczik, K., Lazzari, V., de Vos, J., Kullmer, O., Schrenk, F., Hublin, J.J., Jacob, T., Tafforeau, P., 2009. Taxonomic assessment of the Trinil molars using non-destructive 3D structural and development analysis. PaleoAnthropol. 2009, 117–129.
Smith, T.M., Olejniczak, A.J., Martin, L.B., Reid, D.J., 2005. Variation in hominoid molar enamel thickness. J. Hum. Evol. 48, 575–592.
Smith, T.M., Olejniczak, A.J., Reid, D.J., Ferrell, R.J., Hublin, J.J., 2006. Modern human molar enamel thickness and enamel-dentine junction shape. Arch. Oral Biol. 51, 974–995.
Smith, T.M., Olejniczak, A.J., Zermeno, J.P., Tafforeau, P., Skinner, M.M., Hoffmann, A., Radovčić, J., Toussaint, M., Kruszynski, R., Menter, C., Moggi-Cecchi, J., Glasmacher, U.A., Kullmer, O., Schrenk, F., Stringer, C., Hublin, J.-J., 2012. Variation in enamel thickness within the genus *Homo*. J. Hum. Evol. 62, 395–411.
Smith, T.M., Reid, D.J., Dean, M.C., Olejniczak, A.J., Martin, L.B., 2007. Molar development in common chimpanzees (*Pan troglodytes*). J. Hum. Evol. 52, 201–216.
Spassov, N., Geraads, D., Hristova, L., Markov, G.N., Merceron, G., Tzankov, T., Stoyanov, K., Böhme, M., Dimitrova, A., 2012. A hominid tooth from Bulgaria: the last pre-human hominid of continental Europe. J. Hum. Evol. 62, 138–145.
Spoor, C.F., Zonneveld, F.W., Macho, G.A., 1993. Linear measurements of cortical bone and dental enamel by computed tomography: applications and problems. Am. J. Phys. Anthropol. 91, 469–484.
Suwa, G., Kono, R.T., Simpson, S.W., Asfaw, B., Lovejoy, C.O., White, T.D., 2009. Paleobiological implications of the *Ardipithecus ramidus* dentition. Science 326, 94–99.
Szalay, F.S., Delson, E., 1979. Evolutionary History of the Primates. Academic Press, New York.
Ungar, P.S., 1996. Dental microwear of European Miocene catarrhines: evidence for diets and tooth use. J. Hum. Evol. 31, 335–366.
Winkler, L.A., Schwartz, J.H., Swindler, D.R., 1991. Aspects of dental development in orangutan prior to the eruption of the permanent dentition. Am. J. Phys. Anthropol. 86, 255–271.
Wood, B.A., Harrison, T., 2011. The evolutionary context of the first hominins. Nature 470, 347–352.
Zanolli, C., 2014. Molar crown inner structural organization in Javanese *Homo erectus*. Am. J. Phys. Anthropol., http://dx.doi.org/10.1002/ajpa.22611.
Zanolli, C., Bondioli, L., Coppa, A., Dean, M.C., Bayle, P., Candilio, F., Capuani, S., Dreossi, D., Fiore, I., Frayer, D.W., Libsekal, Y., Mancini, L., Rook, L., Medin Tekle, T., Tuniz, C., Macchiarelli, R., 2014. The late Early Pleistocene human dental remains from Uadi Aalad and Mulhuli-Amo (Buia), Eritrean Danakil: macromorphology and microstructure. J. Hum. Evol. 74, 96–113.
Zanolli, C., Mazurier, A., 2013. Endostructural characterization of the *H. heidelbergensis* dental remains from the early Middle Pleistocene site of Tighenif, Algeria. C.R. Palevol 12, 293–304.
Zanolli, C., Rook, L., Macchiarelli, R., 2010. Analyse structurale à haute résolution des dents de *Oreopithecus bambolii*. Ann. Univ. Ferrara Mus. Sci. Nat. 6, 69–76.
Zhang, L.Z., Zhao, L.X., 2013. Enamel thickness of *Gigantopithecus blacki* and its significance for dietary adaptation and phylogeny. Acta Anthropol. Sin. 32, 365–376.